A radio-frequency nonequilibrium atmospheric pressure plasma operating with argon and oxygen

M. Moravej, X. Yang, and R. F. Hicks[a)]
Chemical Engineering Department, University of California, Los Angeles, California 90095

J. Penelon and S. E. Babayan
Surfx Technologies LLC, 3617 Hayden Avenue, Culver City, California 90232

(Received 20 April 2005; accepted 15 March 2006; published online 15 May 2006)

A capacitively coupled, atmospheric pressure plasma has been developed that produces a high concentration of reactive species at a gas temperature below 300 °C. The concentration of ground-state oxygen atoms produced by the discharge was measured by NO titration, and found to equal 1.2 vol %, or $1.2\pm0.4\times10^{17}$ cm^{-3}, using 6.0 vol % O_2 in argon at 150 W/cm^3. The ozone concentration determined at the same conditions was $4.3\pm0.5\times10^{14}$ cm^{-3}. A model of the gas phase reactions was developed and yielded O atom and O_3 concentrations in agreement with experiment. This plasma source etched Kapton® at 5.0 μm/s at 280 °C and an electrode-to-sample spacing of 1.5 cm. This fast etch rate is attributed to the high O atom flux generated by the plasma source.
 [DOI: 10.1063/1.2193647]

I. INTRODUCTION

Oxygen plasmas have numerous applications for etching, cleaning, sterilization, surface modification, and thin film deposition.[1] The majority of plasmas used in industrial applications operate either in vacuum (<1.0 Torr) or at atmospheric pressure. Atmospheric discharges have the advantage of treating three-dimensional objects and can be used for continuous in-line processing.[2,3] These plasmas are characterized by whether the neutral molecules approach thermal equilibrium with the free electrons. Thermal plasmas, or arcs, exhibit gas temperatures exceeding 2000 °C,[4] while nonequilibrium discharges operate at neutral gas temperatures below 500 °C.[5]

There is great interest in nonequilibrium atmospheric pressure discharges, as evidenced by the many symposia devoted to this topic over the past five years.[6] These sources are increasingly being used for materials processing in the semiconductor, biomedical, automotive, and aerospace industries. Examples of nonequilibrium atmospheric pressure plasmas include coronas,[5,7] dielectric barrier discharges (DBDs),[8–12] microhollow cathode discharges,[13,14] and noble-gas stabilized, capacitive discharges.[3,15–17] Coronas and DBDs were introduced decades ago and have been studied extensively. On the other hand, microhollow cathode and capacitive discharges have not been examined as extensively.

Herein, we report on a low temperature, atmospheric pressure plasma that operates with radio frequency power at 13.56 MHz and produces 1.2 vol % oxygen atoms. The current and voltage waveforms indicate that it is a capacitive discharge. This source produces a high flux of oxygen atoms that etch Kapton® at very fast rates, >1.0 μm/s. Below we describe the physics and chemistry of this plasma source.

[a)]Electronic mail: rhicks@ucla.edu

II. EXPERIMENTAL METHODS

A schematic of the experimental apparatus is shown in Fig. 1(a). The plasma source consisted of a quartz tube, 2.0 mm inside diameter and 1.0 mm wall thickness, which was mounted between two parallel aluminum electrodes. One of the electrodes was supplied with radio frequency power at 13.56 MHz, while the other one was grounded. Argon and oxygen gas flowed through the quartz tube, where they were broken down to generate the discharge. Shown in Fig. 1, parts (b) and (c), are two pictures of the plasma source, with a Kapton® film, 50 μm thick, placed about 1.5 cm downstream of the electrodes. The bright white glow is of the plasma generated in the tube between the electrodes, which were 10 cm long. In (b), the gas was pure argon, and one can see that it does not penetrate the film. However, in (c), 2.0 vol % O_2 was added to the argon, and the discharge has punched a hole ~4 mm in diameter through the film. It took much less than a minute for the hole to appear in the Kapton®.

A tuned impedance probe (Advanced Energy RFZ 60) was inserted between the plasma source and the matching network. The plasma voltage as a function of current and the delivered power were determined with the advanced energy probe, which also yielded information on the impedance, resistance, and phase angle. To determine the time-dependent current and voltage (*IV*) wave forms, an *IV* probe was placed in the line between the impedance probe and the plasma source. This probe was connected to an oscilloscope (Tektronix, TDS 224) that had a 5.0 ns time resolution. The operating conditions of the plasma were: 5.0 L/min Ar, 6.0 vol % O_2, and 150 W/cm^3. This power density reported is the one that is measured by the impedance probe therefore it is the total delivered power and not only the plasma power.

The gas temperature of the argon/oxygen discharge was determined by adding 0.001 L/min N_2 to the gas mixture, and performing optical emission spectroscopy (OES). The

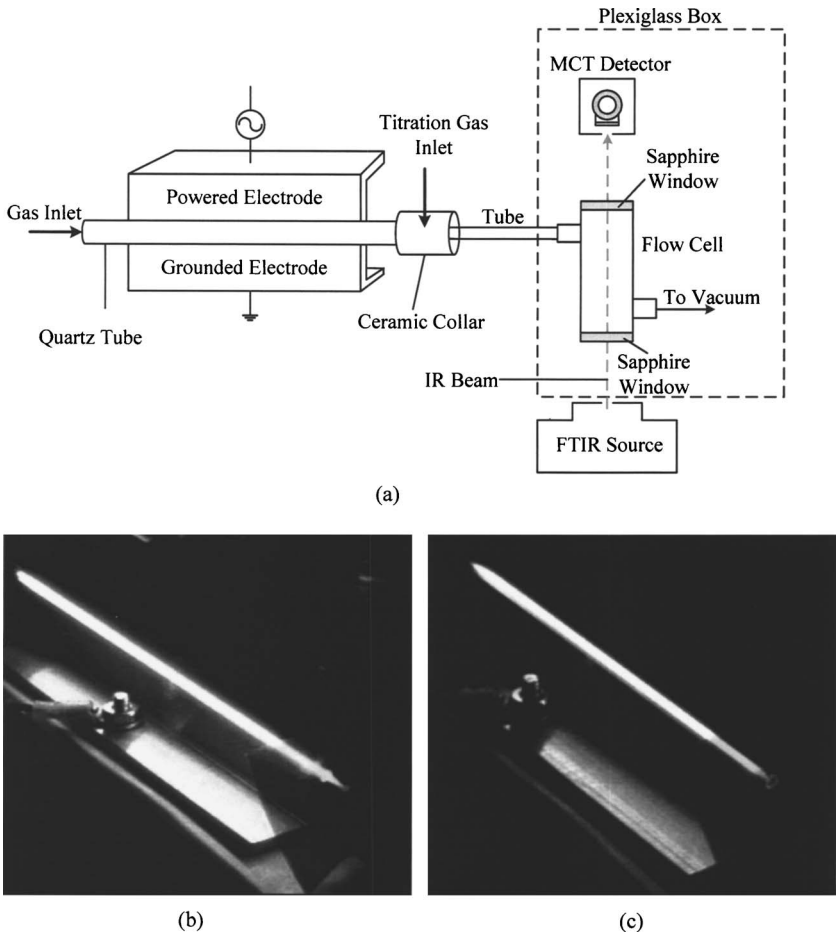

FIG. 1. (Color online) (a) Schematic of the experimental apparatus (not drawn to scale); (b) picture of the plasma source fed with pure argon; and (c) picture of the plasma source fed with argon and 2.0 vol.% O_2.

light was collected with a fiber optic cable that was attached to a monochromator (Instruments S.A., Triax 320). The monochromator was equipped with a 1200 groove/mm grating and a liquid-nitrogen-cooled charge-coupled device (CCD) (Instruments S.A., CCD-3000). A slit width of 0.3 mm was used resulting in a spectral resolution of 0.14 nm. To measure the gas temperature, the rotational temperature of the (3,0) band of the N_2 first positive emission spectrum was fitted to the Boltzmann plot.[18]

The concentration of the ground-state oxygen atoms was determined by titration with nitric oxide (NO), which produced nitrogen dioxide (NO_2).[19] For these experiments, a ceramic collar was inserted on the end of the quartz tube. This ceramic collar had a small opening, 0.5 cm downstream of the plasma, through which the NO was introduced. Another tube connected the gas effluent to a flow cell that was pumped at the other end as shown in Fig. 1. A Fourier-transform infrared spectrometer (BioRad FTS-7) was used to monitor the titration process. The infrared beam passed through the flow cell that was fitted with KBr windows. The light was collected with a mercury-cadmium-telluride (MCT) detector at a resolution of 1 cm^{-1} and by signal averaging 64 scans.

The ozone concentration was determined in the afterglow of the plasma by ultraviolet absorption spectroscopy. The same apparatus was used as that shown in Fig. 1, except that the FTIR source was replaced by a mercury lamp, and the light was collected with a CCD. The average absolute concentration of ozone in the plasma afterglow was calculated from the reduction in the Hg I emission intensity at 253.7 nm. It is noted that the absorption cross-section of O_3 at this wavelength, 1.16×10^{-17} cm^2, is much larger than the absorption cross-section of the weak Herzberg continuum of O_2, $<1\times10^{-23}$ cm^2.[20–22]

III. RESULTS

The root mean square values for the current and voltage wave forms for an argon discharge with 6.0 vol % O_2 at 150 W/cm^3 are shown in Fig. 2. The peak values of the current and the voltage are 3.5 A and 1582 V, respectively. Both curves are sinusoidal and the current leads the voltage by 89.5°. This phase angle indicates that the discharge is

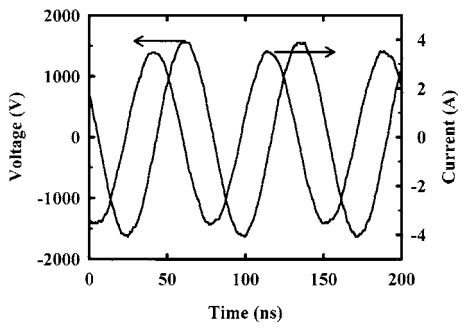

FIG. 2. (Color online) Current and voltage waveforms for argon and 6.0 vol.% O_2.

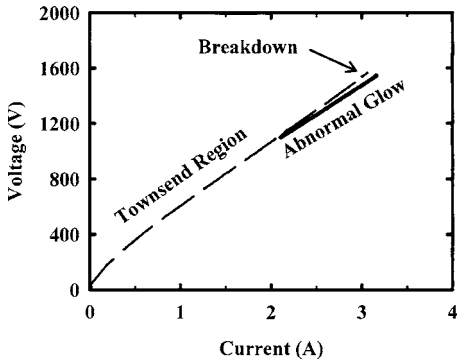

FIG. 3. (Color online) Voltage as a function of current for an argon discharge fed with 1.0 vol.% O_2.

capacitive. The 1° phase shift is caused by the resistive nature of the plasma.[23] The current curve does not contain any spikes due to the charging and discharging of the quartz. This indicates that this plasma source does not behave like a dielectric barrier discharge.[8–12]

A current-voltage curve for the argon plasma operated with 1.0 vol % oxygen is shown in Fig. 3. The dashed curve represents the Townsend region, where the voltage increases linearly with the current, and the discharge has not yet been struck. The gas breaks down at 3.1 A and 1566 V, after which the current and voltage drop to 2.2 A and 1137 V, respectively. Raising the power further causes the current and voltage to increase following a trend characteristic of an abnormal glow discharge.[1] The plasma was turned off at the end of the solid curve to avoid any damage to the impedance probe due to the high voltages.

Shown in Fig. 4 is the dependence of the infrared peak height of NO_2 at 1627 cm^{-1} as a function of the NO feed concentration. The plasma conditions were 5.0 L/min Ar, 6.0 vol % O_2, 150 W/cm^3, and a gas temperature of 300±30 °C (as measured by spectroscopic methods). The peak intensity increased linearly with the NO concentration up to 1.0×10^{17} cm^{-3}, and thereafter it remained relatively constant. A plateau is observed at the point where the O atom concentration begins to limit the rate of production of NO_2. Since the reaction stochiometry between O and NO is 1:1, the knee in the curve corresponds to the point where the nitric oxide concentration equals that of the oxygen atoms. This value was $1.2\pm0.4\times10^{17}$ cm^{-3}. At the plasma conditions, the gas density was 1.3×10^{19} cm^{-3}, which means that the oxygen atoms make up 1.2 vol % of the total gas. The percent dissociation of the oxygen molecules is 16.0%.

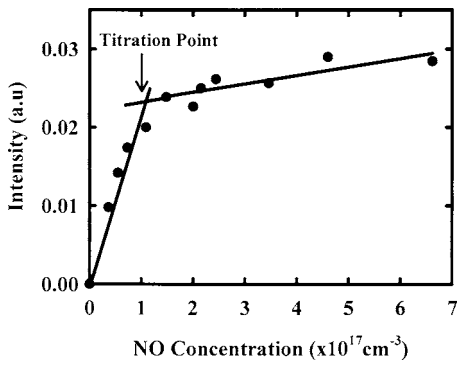

FIG. 4. (Color online) The dependence of the NO_2 infrared peak intensity on the NO feed concentration in the afterglow.

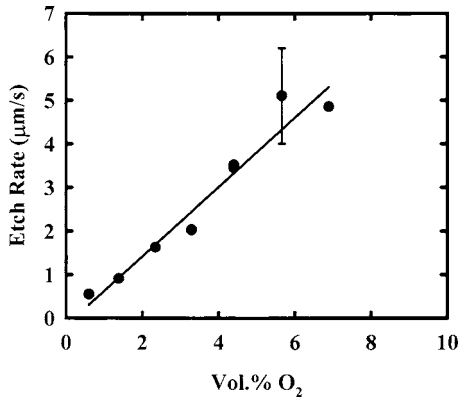

FIG. 5. (Color online) The dependence of the Kapton® etch rate on the O_2 feed concentration to the plasma.

The ozone concentration was determined using UV absorption, as described above. The change in the Hg I peak intensity at 253.7 nm was measured with the plasma on and off. When the plasma was on, the peak intensity was reduced due to the absorption of the light. It should be noted that these experiments were repeated with a pure argon plasma, and it was found that the discharge did not change the Hg I peak height appreciably. The O_3 concentration was found to be $4.3\pm0.5\times10^{14}$ cm^{-3}.

The plasma source was used to etch Kapton® films, and the results are presented in Fig. 5. The operating conditions used in these experiments were 5.0 L/min Ar, 150 W/cm^3, 1.5 cm electrode-to-sample spacing, and a gas temperature of 280±30 °C. The Kapton® film was 50 μm thick and the etch rate was measured by determining the time it took the plasma to punch a hole through the film. The etch rate increased with the O_2 feed concentration from 0.5 μm/s at 1.0 vol % to about 5.0 μm/s at 6.0–7.0 vol %. The O_2 feed was not increased beyond 7.0 vol % because more power would be needed to fill the entire discharge volume. No etching was observed with a pure argon plasma at 150 W/cm^3 and 280 °C. The high etch rates achieved with this plasma source are most likely due to the high flux of O atoms at the substrate surface.[15,16]

IV. DISCUSSION

The plasma density and electron temperature were calculated for the plasma fed with 5.0 L/min Ar and 6.0 vol % O_2. The quartz consumes part of the supplied voltage so to account for it the following formula was used[24]

$$V_0 = \varepsilon V, \tag{1}$$

where, V is the plasma voltage, V_0 is the supplied voltage, and ε is the dielectric constant of quartz, which equals 4.2. The plasma voltage, V, calculated from this equation is the voltage across the inner diameter of the quartz tube on either side. Once the voltage is calculated, it is inserted into the following equation to determine the sheath thickness.[1]

$$J = 1.68\varepsilon_0 \left(\frac{2e\lambda_i}{M}\right)^{1/2} \frac{V^{3/2}}{s^{5/2}}. \tag{2}$$

Here, J is the current density (A/m^2), ε_0 is the permittivity of vacuum (F/m), e is a unit charge (C), M is the molecular weight of the most abundant ion, O_2^+ (kg/mol), λ_i is the mean free path of the ion (m), and s is the total sheath thickness (m). From the sheath thickness, the sheath capacitance can be calculated from[1]

$$C = \frac{1.52\varepsilon_0 A}{s}, \tag{3}$$

where A is the electrode area (m^2). Finally, the voltage drop across the sheath is given by:

$$V_S = \frac{I}{2\pi f C}, \tag{4}$$

where f is the frequency (Hz). Once the voltage drop across the sheath and its thickness are calculated, the bulk plasma parameters can be determined and used to calculate the electron density and temperature. It should be noted that the sheath will most likely not be cylindrical in shape but will just occupy an area around the edges of the quartz that are in contact with the electrodes. However, the sheath values are calculated from a one-dimensional analysis, and are therefore approximate.

The plasma density was calculated from the following equation:

$$J = -en_e\mu_e E, \tag{5}$$

where J is the current density (A/m^2), e is a unit charge (C), μ_e is the electron mobility (V/m s, which is inversely proportional to the pressure), E is the bulk electric field (V/m), and n_e (m^{-3}) is the electron density. The average electron temperature is calculated from a steady-state power balance on the free electrons in the plasma.[17,25]

$$\eta = n_e \frac{P}{K_B T_g} k_1 I_1 + n_e \left[n_e \langle \sigma_{ei} \upsilon_e \rangle + \frac{P}{K_B T_g} \langle \sigma_{ea} \upsilon_e \rangle \right] \frac{2m_e}{M} \frac{3}{2} K_B (T_e - T_g) - \eta_{\text{radiation}}. \tag{6}$$

Here η is the power density (W/m^3), P is the pressure (Pa), T_g is the gas temperature (eV), T_e is the electron temperature (eV), k_1 is the ionization rate coefficient (which is a function of T_e), I_1 is the first ionization energy (eV), $\langle \sigma_{ei} \upsilon_e \rangle$ and $\langle \sigma_{ea} \upsilon_e \rangle$ are the electron-ion and electron-atom collision rate coefficients (which are functions of n_e and T_e), and $\eta_{\text{radiation}}$ is the energy loss due to radiation, respectively. The energy loss due to radiation was estimated using the method described by Benoy *et al.*[26] This term only affected the T_e value by approximately 1.0%. The details of these equations have been published elsewhere.[17]

For the argon plasma fed with 6.0 vol % O_2 at 150 W/cm^3 and 300 °C gas temperature, the delivered voltage and current were 1540 V and 3.3 A, respectively. These values lead to a sheath thickness and voltage drop of approximately 0.04 mm and 1130 V, and a bulk electric field of 80 kV/m. It should be noted that with this potential, which applies only to the plasma and not the entire electrode gap, the power density was calculated to be 110 W/cm^3. From these parameters, a plasma density and electron temperature of 4.4×10^{12} cm^{-3} and 1.2 eV were calculated. These values of the n_e and T_e may vary throughout the plasma and these calculated numbers are the averages that represent the plasma as a bulk.

Using n_e, T_e, gas temperature, and kinetic data obtained from the literature, a model of the plasma was developed to predict the concentration profiles of each species. The reaction mechanism is given in Table I. The predicted profiles of O, $O_2(^1\Delta_g)$, O_3, O_2^+, O_2^-, O^-, O^+, Ar^*, Ar_2^+, and Ar^+ in the plasma are shown in the shaded region of Fig. 6. The concentration of $O(^1D)$ dropped rapidly to a negligible amount so it is omitted from the graph. An initial concentration of 7.7×10^{17} cm^{-3} of O_2 was input into the model, which corresponds to 6.0 vol %. The initial concentration of all the other species was zero. The end of the plasma is at a distance of 10.2 cm, corresponding to a time of 1.85 ms. At the end of the discharge the concentrations of O, $O_2(^1\Delta_g)$, O_3, O_2^+, O_2^-, O^-, O^+, Ar^*, Ar_2^+, and Ar^+ are 1.4×10^{17}, 1.8×10^{16}, 1.0×10^{15}, 4.3×10^{12}, 2.8×10^{12}, 1.9×10^{11}, 2.0×10^{10}, 2.9×10^{9}, 3.1×10^{8}, and 1.8×10^{8} cm^{-3}, respectively. It can be seen that the ground-state O atoms are the most abundant reactive intermediates in the plasma. The concentrations of the negative species in the plasma (the electrons and O_2^-) equals 7.1×10^{12} cm^{-3}, while the concentration of the positive ions is 4.3×10^{12} cm^{-3}. Therefore, to within the uncertainty of the rate constants, the plasma is quasineutral.

Reactions 2, 24–26, 28–31, and 42–47 in Table I were used to develop a model for the afterglow. The concentration of electrons and ions in the afterglow was considered to be negligible. To estimate the lifetime of electrons in the afterglow, reactions 3, 4, 19–21, 38, and 39 in Table I were used to create an approximate model. It was found that the electrons reach an insignificant concentration ($<10^6$ cm^{-3}) in less than 0.1 ms. Jeong *et al.*[16] performed Langmuir probe measurements on a low temperature, atmospheric pressure plasma and determined the concentration of ions in the plasma afterglow to be $<10^{11}$ cm^{-3}. Therefore, because of their low densities, ions and electrons were not included in the afterglow model. A gas temperature of 300 °C was used in the calculation of the rate constants. The concentrations of O_2, O, O_3, and $O_2(^1\Delta_g)$ out of the plasma were used as initial values in the afterglow model.

The concentration profiles as a function of time and distance in the afterglow are shown in Fig. 6. A time (and distance) of 0.0 corresponds to the exit of the plasma. The titration point is denoted with the vertical dashed line. At the titration point, 0.5 cm downstream of the plasma, the model predicts an O atom density of 1.0×10^{17} cm^{-3}, which is the same to within the experimental error of the measured value of $1.2\pm0.4\times10^{17}$ cm^{-3}. The O_3 concentration was measured by placing the quartz tube into the inlet of the flow cell shown in Fig. 1. This flow cell was 20 cm long and 2.5 cm in diameter, yielding a gas velocity of 0.4 m/s, which is almost two orders of magnitude lower than the gas velocity in the quartz tube. For this reason, Fig. 6 does not show the region where the O_3 concentration was measured. In the model, the

TABLE I. Reactions and rate constants for the oxygen plasma.

	Reaction	Rate Constant (cm^3/s)		Ref.
R_1	$e+O_2 \rightarrow 2O+e$	$4.2\times10^{-9}e^{-5.6/T_e}$		1
R_2	$O+O+M \rightarrow O_2+M$	$5.2\times10^{-35}e^{900/T}$	a	1
R_3	$e+O_2 \rightarrow O^-+O$	$8.8\times10^{-11}e^{-4.4/T_e}$		1
R_4	$e+O_2 \rightarrow O_2^+ +2e$	$9.0\times10^{-10}T_e e^{-12.6/T_e}$		1
R_5	$e+O^- \rightarrow O+2e$	$2.0\times10^{-7}e^{-5.5/T_e}$		1
R_6	$e+O_2^+ \rightarrow 2O$	$\frac{5.2\times10^{-9}}{T_e}$		1
R_7	$e+Ar \rightarrow Ar^+ +e$	$4.0\times10^{-12}T_e^{0.5}e^{-15.8/T_e}$		27
R_8	$e+Ar \rightarrow Ar^* +e$	$1.0\times10^{-11}T_e^{0.75}e^{-11.6/T_e}$		27
R_9	$e+Ar^* \rightarrow Ar^+ +2e$	$6.8\times10^{-9}T_e^{0.67}$		28
R_{10}	$e+Ar_2^+ \rightarrow Ar^* +2e$	$5.4\times10^{-8}T_e^{-0.66}$		28
R_{11}	$2e+Ar^+ \rightarrow Ar^* +2e$	$5.0\times10^{-27}T_e^{-4.5}$	a	29
R_{12}	$Ar^*+Ar^* \rightarrow Ar^+ +Ar+e$	5.0×10^{-10}		27
R_{13}	$Ar^+ +2Ar \rightarrow Ar_2^+ +Ar$	2.5×10^{-31}	a	29
R_{14}	$O^-+O_2^+ \rightarrow O+O_2$	$2.0\times10^{-7}(\frac{300}{T})^{0.5}$		1
R_{15}	$O^-+O \rightarrow O_2+e$	2.0×10^{-10}		1
R_{16}	$O^-+O_2^+ \rightarrow 3O$	1.0×10^{-7}		1
R_{17}	$O_2^-+O_2^+ \rightarrow 2O_2$	$2.0\times10^{-7}(\frac{300}{T})^{0.5}$		1
R_{18}	$O_2^-+O_2^++O_2 \rightarrow 3O_2$	$2.0\times10^{-25}(\frac{300}{T})^{2.5}$		1
R_{19}	$e+O_2 \rightarrow O_2(^1\Delta_g)+e$	$1.7\times10^{-9}e^{-3.1/T_e}$		1
R_{20}	$e+O_2(^1\Delta_g) \rightarrow e+O_2$	$5.6\times10^{-9}e^{-2.2/T_e}$		1
R_{21}	$e+O_3 \rightarrow O_2^- +O$	1.0×10^{-9}		1
R_{22}	$O^-+O_2(^1\Delta_g) \rightarrow O_3+e$	3.0×10^{-10}		1
R_{23}	$O^-+O_2(^1\Delta_g) \rightarrow O_2^- +O$	1.0×10^{-10}		1
R_{24}	$O_3+O_2 \rightarrow 2O_2+O$	$7.3\times10^{-10}e^{-11400/T}$		1
R_{25}	$O_3+O \rightarrow 2O_2$	$1.8\times10^{-11}e^{-2300/T}$		15
R_{26}	$O+O+O_2 \rightarrow 2O_2$	$2.5\times10^{-31}T^{-0.63}$	a	15
R_{27}	$O^-+O_2^++O_2 \rightarrow O_3+O_2$	$2.0\times10^{-25}(\frac{300}{T})^{2.5}$		1
R_{28}	$O+O_2+M \rightarrow O_3+M$	$1.9\times10^{-35}e^{1057/T}$	a	15
R_{29}	$O_3+M \rightarrow O+O_2+M$	$7.3\times10^{-10}e^{-11400/T}$		15
R_{30}	$O+O_2+O_2 \rightarrow O_3+O_2$	$6.9\times10^{-34}(\frac{300}{T})^{1.25}$	a	15
R_{31}	$O_2(^1\Delta_g)+O_3 \rightarrow 2O_2+O$	$6.0\times10^{-11}e^{-2853/T}$		15
R_{32}	$O_2+Ar^* \rightarrow O_2+Ar$	1.1×10^{-9}		30
R_{33}	$O+Ar^* \rightarrow O+Ar$	8.1×10^{-12}		30
R_{34}	$O_2+Ar^* \rightarrow Ar+O+O$	5.8×10^{-11}		30
R_{35}	$O_2+Ar^+ \rightarrow O_2^+ +Ar$	1.2×10^{-11}		31
R_{36}	$O+Ar^+ \rightarrow O^+ +Ar$	1.2×10^{-11}		31
R_{37}	$Ar_2^+ +O_2 \rightarrow O_2^+ +2Ar$	1.0×10^{-10}		32
R_{38}	$e+O_2 \rightarrow O+O(^1D)+e$	$5.0\times10^{-8}e^{-8.4/T_e}$		1
R_{39}	$e+O \rightarrow O(^1D)+e$	$4.2\times10^{-9}e^{-2.25/T_e}$		1
R_{40}	$e+O(^1D) \rightarrow O+e$	8.0×10^{-9}		1
R_{41}	$e+O(^1D) \rightarrow O^+ +2e$	$9.0\times10^{-9}T_e^{0.7}e^{-11.6/T_e}$		1
R_{42}	$O(^1D)+O \rightarrow 2O$	8.0×10^{-12}		1
R_{43}	$O(^1D)+O_2 \rightarrow O+O_2$	$7.0\times10^{-12}e^{67/T}$		1
R_{44}	$O(^1D)+O_2 \rightarrow O+O_2(^1\Delta_g)$	1.0×10^{-12}		1
R_{45}	$O_2(^1\Delta_g)+O_2 \rightarrow 2O_2$	$5.0\times10^{-18}e^{-280/T}$		15
R_{46}	$O_2(^1\Delta_g)+O \rightarrow O_2+O$	1.7×10^{-16}		15
R_{47}	$O_2(^1\Delta_g)+M \rightarrow O_2+M$	8.0×10^{-21}		15

[a]Rate constant is in cm^6/s.

O_3 concentration levels out at about 5.7×10^{14} cm^{-3}. This value is in reasonably good agreement with the measured value of $4.3\pm0.5\times10^{14}$ cm^{-3}.

The plasma source presented herein exhibits a combination of properties that are different from the previously reported atmospheric pressure discharges. From the current and voltage wave forms, it is evident that a capacitive discharge forms that is unlike a dielectric barrier discharges operating at low frequency. These latter discharges consist of planar or concentric metal electrodes where one or both of the electrodes are covered with dielectric material. These sources are driven with ac power at 1–100 kHz (Refs. 10, 11, 33, and 34). Usually DBDs operate in a filamentary or micro-discharge mode.[2] However, when an inert gas such as helium is added, a diffuse glow can be achieved.[10–12,35,36] The current wave forms of these discharges show periodic spikes that are due to the charging and discharging of the dielectric during each cycle.[11] No spikes are seen in the current curve in Fig. 2 that would be indicative of the charging and discharging of the dielectric. In addition, no microarcs or streamers can be discerned in the plasma. Other researchers have observed similar IV behavior for RF powered atmospheric plasmas.[37–39]

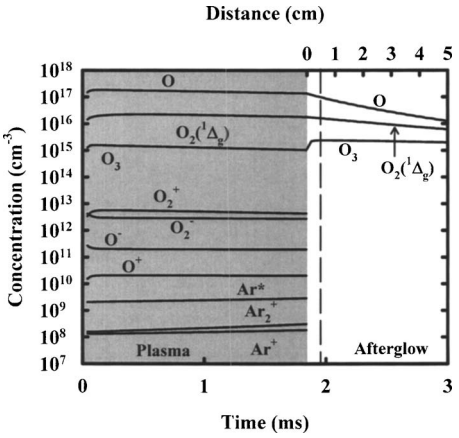

FIG. 6. (Color online) The predicted concentrations of the species in the plasma and afterglow as a function of time and distance.

Another unique property of this atmospheric plasma is the high rate of production of reactive species. There have been several studies on the generation of oxygen atoms in low temperature, atmospheric plasmas.[40–42] It has been predicted that in corona discharges the maximum O atom density at room temperature is 10^{12} cm^{-3} in the plasma and 10^{10} cm^{-3} in the afterglow.[41] To our knowledge there are no experimental measurements of the density of oxygen atoms in DBDs. However, Niessen *et al.*[42] developed a numerical model of a dielectric barrier discharge with a volume of 19.5 cm^3, and a gas feed mixture of N_2, O_2, and H_2O at 100 °C. In this plasma, they calculated a maximum O atom density of 7.0×10^{13} cm^{-3}. Dhali and Sardja[40] modeled the concentration profiles in a single streamer of a DBD, where the n_e was assumed to be on the order of 10^{14} cm^{-3}. The O atom density was estimated to be 5.0×10^{16} cm^{-3}. The oxygen atom density has been determined in a rf capacitive plasma that consisted of parallel aluminum plates separated by a gap of 1.6 mm.[15] The maximum oxygen atom density was found to be 1.0×10^{16} cm^{-3} at 2.5 vol % oxygen in helium, 30.5 W/cm^3, and a gas temperature of 100 °C.[15] This value is ten times less than the O atom density produced by the plasma source reported herein.

We have shown in the past that ground-state oxygen atoms are responsible for etching Kapton®.[15,16] Therefore, the fast rates observed with the present plasma source (cf. Fig. 5) are most likely attributed to the high O atom concentration. In a previous study with an atmospheric pressure plasma jet, a maximum Kapton® etching rate of 8.0 $\mu m/min$ was

achieved at 500 W (62 W/cm^3), 1.3 vol % O_2, 250 °C, and a 5 mm electrode-to-sample spacing.[16] Note that the plasma jet processed a circular spot about 5.0 mm in diameter. This may be compared to the present study, where a spot 2.0 mm in diameter was etched at 5.0 $\mu m/s$ at 280 °C. This source has been scaled up to treat larger areas and has exhibited a similar performance in terms of processing rates, showing that the plasma still produces a high concentration of reactive species. Such a source has numerous applications in surface treatment during electronics packaging, medical device assembly, and the manufacturing of automotive and aerospace products.

V. CONCLUSIONS

We have developed an atmospheric pressure plasma source that operates at a power density of 150 W/cm^3 without forming an arc. At 6.0 vol % O_2 in argon, 150 W/cm^3, and 300 °C this source produces $1.2\pm0.4\times10^{17}$ cm^{-3} ground-state oxygen atoms and etches Kapton® at 5 $\mu m/s$.

ACKNOWLEDGMENTS

This research was supported by a grant from the University of California Discovery program. One of the authors (M.M.) wishes to thank UCLA for a Dissertation Year Fellowship.

[1]M. A. Lieberman and A. J. Lichtenberg, *Principles of Plasma Discharges and Materials Processing* (Wiley, New York, 1994).
[2]B. Eliasson and U. Kogelschatz, IEEE Trans. Plasma Sci. **19**, 1063 (1991).
[3]A. Schütze, J. Y. Jeong, S. E. Babayan, J. Park, G. S. Selwyn, and R. F. Hicks, IEEE Trans. Plasma Sci. **26**, 1685 (1998).
[4]P. Fauchais and A. Vardelle, IEEE Trans. Plasma Sci. **25**, 1258 (1997).
[5]J. S. Chang, P. A. Lawless, and T. Yamamoto, IEEE Trans. Plasma Sci. **19**, 1152 (1991).
[6]Annual International Workshop on Cold Atmospheric Pressure Plasmas: Sources and Applications (unpublished); Annual Workshop on Frontiers in Low Temperature Plasma Diagnostics (unpublished); Annual meeting of the American Vacuum Society, Plasma Science Section 8—Atmospheric and Microdischarges (unpublished); IEEE International Conference on Plasma Science—Industrial, Commercial, and Medical Plasma Applications—High-pressure and Thermal Plasma Processing (unpublished).
[7]M. Goldman and N. Goldman, in *Corona Discharges* Gaseous Electronics Vol. 1, edited by M. N. Hirsh and H. J. Oakam (Academic, New York, 1978).
[8]S. Kanazawa, M. Kogoma, T. Moriwaki, and S. Okazaki, J. Phys. D **21**, 838 (1988).
[9]T. Yokoyama, M. Kogoma, T. Moriwaki, and S. Okazaki, J. Phys. D **23**, 1125 (1990).
[10]U. Kogelschatz, IEEE Trans. Plasma Sci. **30**, 1400 (2002).
[11]I. Radu, R. Bartnikas, G. Czeremuszkin, and M. R. Wertheimer, IEEE Trans. Plasma Sci. **31**, 411 (2003).
[12]N. Gherardi and F. Massines, IEEE Trans. Plasma Sci. **29**, 536 (2001).
[13]K. H. Schoenbach, M. Moselhy, W. Shi, and R. Bentley, J. Vac. Sci. Technol. A **21**, 1260 (2003).
[14]L. Bardos and H. Barankova, Surf. Coat. Technol. **133–134**, 522 (2000).
[15]J. Y. Jeong, J. Y. Park, I. Henins, S. E. Babayan, V. J. Tu, G. S. Selwyn, G. Ding, and R. F. Hicks, J. Phys. Chem. **104**, 8027 (2000).
[16]J. Y. Jeong, S. E. Babayan, A. Schütze, V. J. Tu, J. Y. Park, I. Henins, G. S. Selwyn, and R. F. Hicks, J. Vac. Sci. Technol. A **17**, 2581 (1999).
[17]M. Moravej, X. Yang, G. R. Nowling, S. E. Babayan, J. P. Chang, and R. F. Hicks, J. Appl. Phys. **96**, 7011 (2004).
[18]M. Simek and S. De Benedictis, Plasma Chem. Plasma Process. **15**, 451 (1995).
[19]M. Mozetič, A. Ricard, D. Babič, I. Poberaj, J. Levaton, V. Monna, and U. Cvelbar, J. Vac. Sci. Technol. A **21**, 369 (2003).
[20]E. C. Y. Inn and Y. J. Tanaka, J. Opt. Soc. Am. **43**, 870 (1953).
[21]E. Vigroux, Ann. Phys. **8**, 709 (1953).
[22]J. Malicet, J. Brion, and D. Daumont, Chem. Phys. Lett. **158**, 293 (1989).
[23]J. W. Nilsson and S. A. Riedel, *Electric Circuits* (Prentice-Hall, Englewood Cliffs, NJ, 2000).
[24]H. D. Young, *University Physics* (Addidon-Wesley, Reading, MA, 1992).
[25]M. Mitchner and C. H. Kruger, Jr., *Partially Ionized Gases* (Wiley, New York, 1973).
[26]D. A. Benoy, J. A. M. Van der Mullen, and D. C. Schram, J. Phys. D **26**, 1408 (1993).
[27]J. W. Shon and M. J. Kushner, J. Appl. Phys. **75**, 1883 (1994).
[28]M. J. McCaughey and M. J. Kushner, J. Appl. Phys. **69**, 6952 (1991).
[29]A. N. Bhoj and M. J. Kushner, J. Phys. D **37**, 2510 (2004).
[30]A. Lebéhot, J. Kurzyna, V. Lago, M. Dudeck, and M. Nishida, Phys. Plasmas **6**, 4750 (1999).
[31]F. Howorka, J. Chem. Phys. **68**, 804 (1978).
[32]J. W. Keto, C. F. Hart, and C. Kuo, J. Chem. Phys. **74**, 4433 (1981).
[33]X. T. Deng and M. G. Kong, IEEE Trans. Plasma Sci. **32**, 1709 (2004).
[34]L. Dong, Z. Mao, Z. Yan, and J. Ran, Appl. Phys. Lett. **84**, 5142 (2004).
[35]N. Gheradi, S. Martin, and F. Massines, J. Phys. D **33**, L104 (2000).
[36]T. C. Montie, K. Kelly-Wintenberg, and J. R. Roth, IEEE Trans. Plasma Sci. **28**, 41 (2000).
[37]T. Shirafuji, T. Kitagawa, T. Wakai, and K. Tachibana, Appl. Phys. Lett. **83**, 2309 (2003).
[38]S. Y. Moon, W. Choe, and B. K. Kang, Appl. Phys. Lett. **84**, 188 (2004).
[39]J. Castro, M. H. Guerra-Mutis, and H. J. Dulce, Plasma Chem. Plasma Process. **23**, 297 (2003).
[40]S. K. Dhali and I. Sardja, J. Appl. Phys. **69**, 6319 (1991).
[41]C. Soria, F. Pontiga, and A. Castellanos, Plasma Sources Sci. Technol. **13**, 95 (2004).
[42]W. Niessen, O. Wolf, R. Schruft, and M. Neiger, J. Phys. D **31**, 542 (1998).